A Neural Network Atmospheric Model for Hybrid Coupled Modelling

by

Youmin Tang, William W. Hsieh, Benyang Tang

Oceanography/EOS

University of British Columbia, Vancouver, B.C., Canada V6T 1Z4

Keith Haines

Department of Meteorology, University of Edinburgh

The King's Buildings, Edinburgh EH9 3JZ, United Kingdom

August 15, 2000

Abstract

The possibility of using a nonlinear empirical atmospheric model for hybrid coupled atmosphere-ocean modelling has been examined by using a neural network (NN) model for predicting the contemporaneous wind stress field from the upper ocean state. Upper ocean heat content (HC) from a 6-layer ocean model was a better predictor of the wind stress than the (observed or modelled) sea surface temperature (SST). Our results showed that the NN model generally had slightly better skills in predicting the contemporaneous wind stress than the linear regression (LR) model in the off-equatorial tropical Pacific and in the eastern equatorial Pacific. When the wind stresses from the NN and LR models were used to drive the ocean model, slightly better SST skills were found in the off-equatorial tropical Pacific and in the eastern equatorial Pacific when the NN winds were used instead of the LR winds. Better skills for the model HC were found in the western and central equatorial Pacific when the NN winds were used instead of the LR winds. Why NN failed to show more significant improvement over LR in the equatorial Pacific for the wind stress and SST is probably because the relationship between the surface ocean and the atmosphere in the equatorial Pacific over the seasonal time scale is almost linear.

1 Introduction

Within the last decade, many models have been developed for forecasting the El Niño-Southern Oscillation (ENSO) phenomena, a coupled atmosphere-ocean interaction centred in the tropical Pacific (Barnston et al., 1994 and Latif et al., 1994). These models are generally classified into three groups: dynamical coupled models, statistical models and hybrid coupled models.

A hybrid-coupled model (HCM) connects a statistical atmospheric model to a dynamical ocean model (Latif and Villwock 1990; Syu et al. 1995; Barnett et al. 1993; Balmaseda et al. 1994). This design uses the fact that the ocean has the long-term memory in the coupled atmosphere-ocean system. The fast adjustment of the atmosphere to the ocean variables such as the sea surface temperature (SST) and upper ocean heat content (HC) motivates the use of a steady-state statistical model for the atmosphere. All HCMs are based on the assumption that for monthly or longer time scales, contemporaneous correlation between wind stress and oceanic variables is associated with the atmosphere's rapid non-local adjustment to the oceanic anomaly patterns throughout the basin (Syu et al.1995). The main advantages of an HCM are: (1) easier understanding of the coupling mechanisms and lower computing cost than a fully coupled GCM (Blanke et al 1997); (2) performing comparable to or even better than a coupled GCM in simulation and prediction (Palmer et al 1994).

An important aspect affecting the HCM performance is the construction of the empirical atmospheric model, e.g. what method was used for estimating the surface wind stress field from a given ocean state, and which oceanic variables were used as predictors for the wind stress. The methods used have advanced from correlation (Latif and Villwock 1990, Latif and Flügel 1991), linear regression with EOF modes (Barnett et al. 1993) to SVD (Singular Value Decomposition) (Syu et al.1995). However, all empirical atmospheric models used in HCMs have so far been linear statistical models. Hence in this paper, we investigate the possibility of improving the empirical atmospheric model by a nonlinear approach using neural networks. Hsieh and Tang (1998) gave a review on the recent applications of neural network models to prediction and data analysis in meteorology and oceanography.

This paper is structured as follows: Section 2 briefly describes the dynamical ocean model. Section 3 describes the empirical atmospheric models, including linear and non-linear models. Section 4 compares the wind stress estimated using the linear and nonlinear models. Section 5 compares the the ocean model forced with the wind stress from the two empirical atmospheric models.

2 Ocean Model

The ocean model used in this research, one of intermediate complexity, originated from Anderson and McCreary (1985) and Balmaseda et al. (1994, 1995), but extended to six active layers in this study. It consists of depth averaged primitive equations in six active layers, overlying a deep inert layer. The model allows for an exchange of mass, momentum and heat at each layer interface by a parameterisation of entrainment. The model uses an Arakawa C grid layout, with a resolution of 1.5^o x 1.5^o, covering an extension from 30°N - 30°S in latitude and from 123°E - 69°W in longitude. The time step for integration is two hours. The boundaries are closed, with free slip conditions.

The model was first spun up for 100 years with monthly climatological FSU (Florida State University) wind stress (Goldenberg and O'Brien 1981) and heat flux Q_s as forcing fields, where

Q_s is represented by the Oberhuber (1988) heat flux Q_0 plus a relaxation term to T_0, the observed SST, i.e.

$$Q_s = Q_0 + \lambda(T - T_0), \tag{1}$$

where T is the model SST, Q_0 and T_0 are the monthly climatological heat flux and SST, respectively, and λ (which is negative) controls the rate of relaxation to the observed SST.

After the 100-year spinup by the seasonal forcing, the model seasonal climatology was obtained. We then made a 30-year model control run, with forcing by the FSU wind stress from 1961-1990. The performance of the model is shown in Table 1 for various regions (Fig.1). Model outputs such as SST and HC would further be used as predictors for the atmospheric model. As done in Balmaseda et al. (1994), for this 30-year integration the surface heat formulation was modified to

$$Q_s = Q_0 + \lambda(T_m - T_0) + 0.2\lambda(T - T_m), \tag{2}$$

where T_m represents the model SST climatology.

3 Atmospheric models

a EOFs for predictors and predictands

Two empirical atmospheric models were constructed: One was the traditional linear regression (LR) model widely used in HCMs (Barnett et al 1993); the other was a non-linear regression model, by neural networks.

As potential predictors for both atmospheric models, several oceanic variables were chosen, namely the observed SST, the model SST and HC from the ocean model forced with the observed wind stress. The time period taken for the model construction was from 1964-1990, since in the first 3 years, the output of the ocean model was greatly affected by the ocean initial conditions and had poor agreement with observations. The observed SSTs were from the Comprehensive Ocean Atmosphere Data Set (COADS, Slutz et al 1985). The FSU wind stress was also detrended by Singular Spectral Analysis (Gill and Vautard, 1991) and smoothed with a 3-month running mean filter.

As in other studies (Barnett et al 1993, Balmaseda 1994), an EOF (Empirical Orthogonal Function) analysis was first applied to each dataset to extract the predictors and predictands. The oceanic predictor field $T(\mathbf{x},t)$, and the predictand field $\tau(\mathbf{x},t)$, the zonal or meridional component of the wind stress, were expressed by EOF analysis as

$$T(\mathbf{x},t) = \sum_n \alpha_n(t)e_n(\mathbf{x}) \qquad\qquad \tau(\mathbf{x},t) = \sum_n \beta_n(t)f_n(\mathbf{x}), \tag{3}$$

where n is the mode number and the seasonal cycle had been removed for both fields prior to the EOF analysis. For the model SST and HC, the first 3 EOF modes accounted for over 70% of total variance, whereas for the observed SST about 67% of total variance was explained by the first 3 zonal EOF modes. In contrast, the first 3 wind stress EOFs explained only 35% of the total variance, due to presence of high frequency oscillations and noise in the wind stress field. The first three zonal wind EOF modes still captured the main low frequency signals, e.g. ENSO, and are highly correlated with the observed SST anomaly averaged over the NINO 3 area (not shown).

All variables have a common feature from their EOF analysis, i.e. the variance contribution by individual modes became rather small after the first 3 modes. Hence, following the suggestions of Latif et al (1990) and Goswami and Shukla (1991), we used the first 3 EOF modes of oceanic variables T as predictors, and the first 3 EOF modes of zonal or meridional wind stress as predictands, in constructing both the linear and the non-linear models. The linear regression model is similar to that of Barnett et al (1993).

b Neural Network Model

A feed-forward neural network (NN) is a non-parametric statistical model for extracting nonlinear relations in the data. A common NN model configuration is to place between the input and output variables (also called 'neurons'), a layer of 'hidden neurons' (Fig.2). The value of the jth hidden neuron is

$$y_j = \tanh(\sum_{\mathrm{i}} \mathrm{w_{ij}x_i} + \mathrm{b_j}), \tag{4}$$

where x_i is the i-th input, w_{ij} the weight parameters and b_j the bias parameters. The output neuron is given by

$$z = \sum_j \tilde{w}_j y_j + \tilde{b}. \tag{5}$$

A cost function

$$J = \langle (z - z_{obs})^2 \rangle \tag{6}$$

measures the mean square error between the model output z and the observed values z_{obs}. The parameters w_{ij}, $\tilde{w}_j$, b_j and $\tilde{b}$ are adjusted as the cost function is minimized. The procedure, known as network training, yields the optimal parameters for the network. As in Tangang et al (1998a,b), steepest descent with momentum and adaptive learning rates was used during the optimization.

The 3 input neurons were the first 3 EOF time series $\alpha_n(t)$ (either for SST or for HC), and the single output neuron was one of the (zonal or meridional) wind stress EOF time series $\beta_n(t)$, i.e. a separate network was used to predict each of the wind stress modes. There was no time lag between the predictors and the predictand.

One critical element in NN design is the size of the architecture, i.e., the number of hidden neurons. A smaller than optimal network fails to learn all the relevant information from the data, i.e. underfits, whereas a larger than optimal network often ends up learning the noise in the data, i.e. overfits. The strategy we employed to determine the number of hidden neurons was based on cross-validating the correlation skills of the network. A cross-validation procedure involves dividing the data record into several segments, selecting one segment for the test data and the rest for training data. The NN model is built using the training data only, and model predictions are tested on the test data. Next, another segment is selected as the test data, and a new model version is built. This is repeated until the entire data record has been used for testing. The cross-validation scheme ensures that no training data are used for testing the prediction skills, hence the artificial skill associated with the overfitting problem (von Storch and Zwiers, 1999) can be effectively eliminated by the cross-validation scheme.

In this study, the record of 1964-1990 was divided into 3 segments, the first 7 years and the remaining two 10-years periods. We tested different NN models by increasing the number of hidden neurons. Cross-validation skills (correlation and Root Mean Square (RMS) error) were monitored for each network. As the number of hidden neurons increased starting from 1 to 3, the cross-validation skills were enhanced. These skills were little changed as the number of hidden neurons was increased to 4-6. But the skills were greatly degraded with further increase in the number of hidden neurons. Hence we used 3 hidden neurons in the atmospheric model. In the case where both SST and HC are used as predictors, the network had 6 input neurons but still only 3 hidden neurons. Cross validation was also used to choose the the error goal (i.e. the level of J to terminate the optimization) and the maximum number of iterations (epochs) in the training process.

Finally, an ensemble of 25 NNs with random initial parameters were used and the final output of the NN model was actually the ensemble average of the 25 individual model outputs. Ensembles can greatly alleviate the instability problems associated with NN modelling (Hsieh and Tang, 1998).

4 Results from atmospheric models

a The predictors

So far, almost all HCMs used either simulated SST from ocean models or observed SST to estimate the wind stress (Barnett et al 1993; Syu et al.1995). Whether SST is the best predictor for the wind stress is debatable. Observations showed that the SSTs do not reflect the changing subsurface temperatures in the tropical western Pacific, where subsurface temperature anomalies and thermocline displacements have an important role in the ocean-atmosphere coupling processes, (White and Pazan 1987, Latif and Graham 1992). Therefore, using upper ocean heat contents (HC) as predictors might produce higher skills than SST.

HC is defined here as the integral of the temperatures over the first two layers, calculated from

$$HC_i = \frac{h_i(T_i - T_7)}{\sum_{i=1}^{6} H_{init}(i)} \qquad\qquad HC = \sum_{i=1}^{2} HC_i, \tag{7}$$

where T_7 is the temperature of the bottom layer, and $H_{init}(i)$ is the initial thickness of layer i. The actual model depths climatologically monthly averaged over 30 year simulations in top two layers range from 89m to 144m in the first layer and from 134m to 188m in the second layer, with variations in season and in space.

The first EOF modes for the HC, the zonal and meridional wind stress (Fig.3), are the modes associated with the ENSO oscillation– where the HC shifts east-west along the equator (Fig.3a), the zonal wind anomaly develops in the western equatorial Pacific (Fig.3b), and the trade winds show anomalous convergence along the equator (Fig.3c). Because of their ENSO nature, the anomalies in these EOF modes are all mainly confined to within 15°N - 15°S (Fig.3). To explain the anomalies outside this narrow equatorial belt, the second, third, and even higher modes are needed.

Table 2 shows the cross-validated skills attained by the NN and LR models with the observed SST, model SST, model HC, and model SST+HC serving as predictors for the wind stress EOF time series β_n $(n = 1, 2, 3)$. Here $SST + HC$ does not mean combined EOFs, but that their separate EOF time series normalized by the standard deviations are the predictors. HC as predictors generally had the highest skills as expected, whereas both observed SST and model SST generally attained the lowest skills. SST+HC predictors attained lower skills than HC alone. This suggests that the first 3 EOFs of HC have well represented the ocean status, and more SST EOFs as input only bring additional noise and overfitting. For the first zonal wind stress mode, the model SST actually did better than the observed SST, probably because the ocean model acted as a complicated space-time filter, thereby removing some noise in the SST (Latif and Graham 1992). For the other wind stress modes, the model SST did not do as well as the observed SST. In general, NN did not predict the first zonal or meridional wind stress mode much better than LR; only for the second and third modes did NN seem to have an edge over LR. Some small differences between LR and NN can be seen in Fig.4, where the NN curves almost overlap the straight lines, indicating weakly nonlinear relations.

b Prediction skills of the NN and LR models

Since we only tried to predict the first 3 wind stress modes, the prediction skills were often compared in later sections against the wind stress reconstructed from the first 3 EOF modes of the FSU wind stress, which we will refer to as the idealized wind stress. Such a comparison more objectively evaluates the skill of the atmospheric model, as it excludes the noisy higher modes which are not modelled. The correlation map between the idealized wind stress and the FSU wind stress shows that the idealized field is a reasonable representation, especially in the western and central Pacific (not shown).

As the model HC has the best prediction skills for the wind stress, henceforth we will only use the HC as predictor. The reconstructed stress field was obtained by multiplying the predicted EOF time series (either by NN or LR) to the spatial EOF modes. The cross-validated correlation and the sum of squared error (SSE) of the reconstructed stress field from NN model verified against the idealized field were shown in Fig.5 and Fig.6. As seen in Fig.5, for zonal stress, the best skills occurred at the equatorial western and eastern Pacific , whereas the worst occurred off the coast of South America, in the Australian summer monsoon region and in the subtropical North Pacific. The high skill areas are associated with the anomalous SST areas during ENSO events where the response of zonal stress to the ocean status is strong due to active coupling. The lower correlation along the coast of South America might be attributed to the fact that wind-stress is almost 'white' in this region (Goldenberg and O'Brien, 1981, Latif and Flügel 1991). For meridional stress, the highest skills were found in the Intertropical Convergence Zone (ITCZ) and the South Pacific Convergence Zone (SPCZ) areas.

The map of SSE (Fig.6) indicated that the estimation of the amplitude by the NN model was good, especially in eastern Pacific ocean. Large errors only occurred at the ITCZ and SPCZ areas, in contrast to the correlation map (Fig.5), where these two areas have good skills (especially for the meridional stress). The active coupling in these areas induced large anomalous variations in the stress, which generated large amplitude errors even though the phase errors were small, producing good correlations but large SSE.

Differences between the prediction skills of the NN model and the LR model for the period of 1964-1990 are shown in Figs. 7 and 8. The correlation skill differences (Fig.7) between NN and LR were very small, though NN skills were indeed slightly ahead of LR skills in most areas. For the zonal stress (Fig.7a), the NN model outperformed LR in almost the whole subtropical domain of 15°N - 30°N and near the Niño3 region. That the improvements occurred in these regions can be understood from our earlier finding (Table 2) that the NN and the LR had the same skill in predicting the mode 1 zonal stress (Fig.3b), but the NN had an edge over LR for modes 2 and 3. Hence only in regions outside the main anomaly area of mode 1 (i.e. the western equatorial Pacific in Fig.3b) would the NN appear to have slightly better skills than LR, as found in Fig.7a. For the meridional stress (Fig.7b), NN did slightly better in the eastern Pacific away from the equator.

The difference of the SSE between the two models (Fig.8) indicated that the NN model slightly outperformed the LR model for much of the domain except for the western equatorial region of 150°E - 160°W centred at 5°S. The slight advantage of NN over LR is manifested more clearly in the error map (Fig.8) than in the correlation map (Fig.7), suggesting that model nonlinearity may be slightly more useful in estimating the amplitude than in estimating the phase of the wind stress anomalies.

The very small skill differences between NN and LR follows from the fact that the equatorial dynamical system is almost linear, so a nonlinear model does not give much better results than a linear model. Tang et al. (2000) found that with sea level pressure (SLP) as predictors for the SST anomalies, NN slightly outperformed LR in the Niño3 region, but not so in the Niño4 region, suggesting that nonlinearity is quite weak in the eastern-central equatorial Pacific, but even weaker in the western-central equatorial Pacific. Here, Fig.8 and to a lesser extent Fig.7 are consistent with the Tang el al. (2000) finding.

5 The ocean model driven by the empirical wind

a SST skills

To assess the effect of the empirical wind stress from the NN and the LR models on the ocean model, we ran the ocean model twice, with forcing by the two model predicted wind stress during the period 1964-1990. The outputs of the ocean model forced by the idealized wind stress (i.e. the first 3 EOFs of the FSU data) were later used to verify the skills from the empirical wind stress. Fig.9 compares the SST from the ocean model driven by the idealized wind stress with that driven by the full FSU stress, showing a generally close relation, especially in the western and central equatorial Pacific. This justifies the use of the ocean model driven by the idealized stress as the standard for comparing the empirical winds.

Fig.10 shows the skills of the SST from the ocean model forced with the empirical wind stress from the NN model. As seen in the correlation map (Fig.10a), the skill is good, with a correlation of over 0.8 covering much of the whole model domain. The highest skill, up to over 0.9, occurred at the central equatorial Pacific region.

A comparison of ocean models driven by the empirical wind stress from the NN model and that from the LR model was then made. Fig.11a depict the difference in the model SST correlation skills between the NN model and the LR model when they were each verified against the standard SST. For the equatorial western and central Pacific, the difference was negligible. As mentioned earlier, this is probably due to the mainly linear dynamics in the equatorial western and central Pacific. The largest differences occurred in the off-equatorial areas and in the eastern equatorial Pacific, where the NN winds tended to outperform the LR winds. The maximum correlation difference reached 0.34 in the northwest region around 150°E and 15°N. The positive correlation skill areas in the off-equatorial regions of Fig.11a roughly coincided with the positive zonal wind stress skills attained by the NN over LR in Fig.7a. There was no such agreement between Fig.11a and Fig.7a in the eastern equatorial Pacific, where the skill differences between NN and LR were small for the zonal stress, but relatively large for the SST. This could be due to the fact that in equatorial western Pacific, the oceanic response is mainly locally forced by the wind stress, whereas in the eastern Pacific, equatorial Kelvin wave propagation, upwelling and vertical mixing are thought to predominantly control the SST variability (Battisi 1988).

The difference in the SST RMS error between the ocean models driven by the NN and LR wind stress (Fig.11b) generally agreed with Fig.11a, i.e. higher correlation skill areas corresponded with lower RMS error regions, and vice versa.

While the above comparisons were based on the model ocean forced with the idealized wind stress as standard, the comparisons based on the model forced with the FSU stress yielded the same conclusions (not shown). We averaged the model SST forced by the FSU stress, the NN and the LR stress over the Niño 1+2 region, and the whole off-equatorial Pacific in the south (25°S - 15°S, 155°E - 80°W) and in the north (15°N - 25°N, 130°E - 105°W) to get the individual SST indices over these areas. With the ocean model driven by the FSU stress as the comparison standard, the correlation skills for the NN model were 0.38, 0.57 and 0.50 respectively in these 3 areas, compared with correlations of 0.31, 0.51 and 0.41 for the LR model in the same areas.

In summary, using a nonlinear empirical atmospheric model to drive the ocean might bring modest benefits for SST simulation in the off-equatorial tropical regions and in the eastern equatorial Pacific. Improvements in the equatorial western and central Pacific would be unlikely as the dynamics in these regions appeared very nearly linear from other studies (e.g. Tang et al. 2000).

b Heat content Skills

The HC redistribution in western tropical Pacific can lead the evolution of SST anomalies in eastern Pacific and has been known to be an important factor in the evolution of many ENSO episodes. In particular, the HC anomalies over the equatorial band 5°N to 5°S can be a very good precursor for the SST anomalies in the Niño3 region (Zebiak 1989, Latif et at 1992, Balmaseda et al 1994). We therefore examined the HC in the ocean model forced with the wind stress from the NN model and from the LR model. The HC from the ocean model forced with the idealized stress was taken as the verification standard.

The HC skills from the ocean forced with the NN model wind stress was generally better than those with the LR stress for the western Pacific basin, in particular in the western and central Pacific over the equatorial band of 10°N to 10°S (Fig.12). From the ocean model driven by the idealized stress, the HC anomalies averaged over the whole equatorial Pacific (124°E-70°W,5°N-5°S) led the observed Niño3 SST anomalies by 3-4 months (Fig.13). Their correlation were 0.73 and 0.72 with the HC leading by 3 and 4 months respectively. The 3-month lag correlations of the observed Niño3 SST anomalies and the HC index averaged over whole equatorial Pacific for the ocean model forced by the NN wind and by the LR wind did indicate the NN wind to have slightly better skill (0.62 for NN and 0.58 for LR).

6 Conclusions

We have examined the possibility of using a nonlinear empirical atmospheric model for hybrid coupled modelling, by developing a neural network (NN) model for predicting the contemporaneous wind stress field from the ocean state, and comparing the NN model with a linear regression (LR) model. Upper ocean heat content (HC) from an ocean model was found to be a better predictor of the wind stress than the (observed or modelled) SST. Our results showed that the NN model generally had slightly better skills in predicting the contemporaneous wind stress than the simple LR model in the off-equatorial tropical Pacific and in the eastern equatorial Pacific, mainly through better predictions of the second and third wind stress modes.

When the NN and LR model produced wind stresses were used to drive the ocean model, slightly better SST skills were found in the off-equatorial tropical Pacific and in the eastern equatorial Pacific when the NN winds were used instead of the LR winds. Better skills for the model HC were found in the western and central equatorial Pacific when the NN winds were used instead of the LR winds. Since the HC involves the product of the upper ocean temperature with the thickness of the upper ocean, it is a more nonlinear variable than the SST– this may partly explain why the nonlinear NN model, when compared with the LR, generally predicted the HC better than the SST. Because changes in the HC in the western equatorial region can lead to SST anomalies in eastern Pacific, the potential skill improvement for HC by NN could be of interest.

As discussed in Tang et al.(2000), there are several possible reasons why NN failed to show more significant improvements over LR in the equatorial Pacific for wind stress and SST. The first (and the most probable) is that the relation between the surface ocean and the atmosphere in the equatorial Pacific over the seasonal time scale is basically linear, with nonlinear processes playing only minor roles. The linear assumption was also supported by Xue et al(1994).

The second reason is that the data records are not long enough. NN is more capable than LR but the data requirement is also considerably higher. To extract more than the linear rules from the data, longer records of good quality data are needed. As Barnett et al.(1993) built LR models for individual calendar months, we also tested empirical atmospheric models for individual seasons. Although the seasonal approach can include the effect of the different basic states in different seasons of the year, we did not find the overall cross-validated anomaly skills better than the model developed using all data– the tradeoff being that by dividing the data record into seasons, we have even less data to construct each seasonal model.

Finally, the NN model is still a rudimentary one and further improvements in the NN model design is possible. So far, the NN has been used as a nonlinear regression model. Work is underway to develop a NN nonlinear canonical correlation analysis model, which should provide a more optimal connection between the predictor and predictand fields.

Acknowledgements

We are indebted to Dr. D.L.T Anderson and Dr. M.A.Balmaseda for providing their 2-layer model code. This work was supported by grants to W. Hsieh from the Natural Sciences and Engineering Research Council of Canada, and Environment Canada; and by British Council Grant CHI2500134 to K. Haines and Y. Tang.

7 References

Anderson DLT, McCreary JP (1985) Slowly propagating disturbances in a coupled ocean-atmosphere model. J Atmos Sci 42: 615-629

Barnston AG, Coauthors (1994) Long-lead seasonal forecasts-Where do we stand? Bull Amer Meteor Soc 75: 2097-2114

Balmaseda MA, Anderson DLT, and Davey MK (1994) ENSO prediction using a dynamical ocean model coupled to statistical atmospheres. Tellus 46A: 497-511

——, Davey MK, Anderson DLT (1995) Decadal and seasonal Dependence of ENSO prediction skill. J Clim 8: 2705-2715

Barnett TP, Latif M, Graham NE, Flügel M, Pazan S, White W (1993) ENSO and ENSO related predictability, Part1: Prediction of equatorial sea surface temperature with a hybrid coupled ocean-atmosphere model. J Clim 6: 1545-1566

Battisti DS (1988) Dynamics and thermodynamics of a warming event in a coupled tropical atmosphere-ocean model. J Atmos Sci 45: 2889-2919.

Blank B, Neelin JD, Gutzler D (1997) Estimating the effect of stochastic wind stress forcing on ENSO irregularity. J Clim 10: 1473-1486

Davey, MK, Ineson S, Balmaseda MA (1994) Simulation and hindcasts of tropical Pacific Ocean interannual variability. Tellus 46A: 433-447

Gill H, Vartard R (1991) Interdecadal oscillations and the warming trend in global temperature time series. Nature 350: 324-327

Goldenberg B, O'Brien JJ (1981) Time and space variability of tropical pacific wind stress. Mon Wea Rev 109: 1190-1207

Goswami BN, Shukla J (1991) Predictability of a coupled ocean-atmosphere model. J Clim 4: 3-22.

Hsieh WW, and Tang B (1998) Applying neural network models to prediction and analysis in meteorology and oceanography. Bull Amer Meteor Soc 79: 1855-1870.

Latif M, Barnett TP, Cane MA, Flügel M, Graham NE, von Storch H, Xu J-S and S.E.Zebiak (1994) A review of ENSO prediction studies. Climate Dyn 9: 167-179

—–,Biercamp J, von Storch H, McPhaden MJ, Kirk E (1990) Simulation of ENSO-related surface wind anomalies with an atmospheric GCM forced by observed SST. J Clim 3: 509-521.

—–, Flügel M (1991) An Investigation of Short-Range climate predictability in the Tropical Pacific. J Geophys Res 96: 2661-2673.

—–,Graham NE (1992) How much predictive skills is contained in the thermal structure of an Oceanic GCM? J Phys Oceanogr 22: 951-962

—–, Villwock A (1990) Interannual variability as simulated in coupled ocean-atmosphere model. J Mar Syst 1: 51-60

Miller AJ, Barnett TP, Graham NE (1993) A comparison of some tropical ocean models: Hindcast Skill and El Niño Evolution. J Phys Oceanoger 23: 1557-1591

Neelin JD (1990) A hybrid coupled general circulation model for El Niño studies. J Atmos Sci 5: 674-693

Oberhuber JM (1988) An atlas based on COADS dataset: the budgets of heat, buoyancy and turbulence kinetic energy at the surface of the global ocean, Max-Plank-Institute fur Meteorologie, Report No.15

Palmer TN, Anderson DLT (1994) The prospects for seasonal forecasting -A review paper. Q J Roy Met sci 7: 755-793

Slutz R. et al 1985: The Comprehensive ocean-atmosphere data set release. I: Climate Research Program, ERL/NOAA, Boulder,CO,39pp.

Syu H-H, Neelin JD, Gutzler D (1995) Seasonal and Interannual variability in a hybrid coupled GCM. J Clim 9: 2121-2143

Tang B, Hsieh, WW, Monahan AH, and Tangang FT (2000): Seasonal predictions of sea surface temperatures in the tropical pacific—–comparing neural networks and canonical correlation analysis. J Clim 13: 287-293

Tangang FT, Hsieh WW, Tang B (1998a) Forecasting regional sea surface temperatures of the tropic by neural network models, with wind stress and sea level pressure as predictors. J. Geophys.Res 103: 7511-7522

—–, Tang B, Monahan AH, Hsieh WW (1998b) Forecasting ENSO events: a neural network-extended EOF approach. J Clim 11: 29-41

von Storch H, Zwiers FW (1999) Statistical Analysis in Climate Research. Cambridge, Cambridge Univ. Pr., 484pp.

White WB, Pazan SE (1987) Hindcast/forecast of ENSO events based upon the redistribution of observed and model heat content in the western tropical Pacific, 1964-86. J Phys Oceanogr 17: 264-280

Wu D-H, Anderson DLT, Davey MK (1994) ENSO prediction experiments using a simple ocean-atmosphere model. Tellus 49A: 464-480

Xue Y, Cane MA, Zebiak SE, Blumenthal MB (1994) On the prediction of ENSO: a study with a low order Markov model. Tellus 46A: 512-528

Zebiak SE (1989) Oceanic heat content variability and El Niño cycles. J Phys Oceanogr 19: 475-486

8 Figure Caption

Fig.1. Location of the various oceanic regions used in the analysis.

Fig.2. An example of a neural network model, where there are four neurons in the input layer, three in the hidden layer, and one in the output layer. The parameters w_{ij} and $\tilde{w}_j$ are the weights, and b_j and $\tilde{b}$ are the biases. The parameters b_j and $\tilde{b}$ can also be regarded as the weights for constant inputs of value 1.

Fig.3. The first EOF mode for (a) the heat content (HC) from the ocean model driven by the FSU wind stress, (b) the FSU zonal wind stress and (c) the meridional wind stress. Negative contours are shown as dashed curves and zero contours as dotted curves. Contour interval = 0.01.

Fig.4. (a) The first mode of the zonal wind stress plotted as a function of the third mode of the SST, and (b) the second mode of the zonal wind stress versus the first mode of the SST. The observations are shown as dots; the simulated zonal wind stress mode from the NN model is indicated by the small circles and from the LR model by the straight lines.

Fig.5. Cross-validated anomaly correlation between the predicted wind stress by NN (with model HC as predictors) and the idealized wind stress (i.e. the FSU wind stress with only the first 3 EOF modes): (a) zonal stress, and (b) meridional stress. Contour interval=0.1. The seasonal cycle has been removed prior to the analysis, and in all following maps.

Fig.6. The sum of squared error (SSE) of the predicted wind stress by NN verified against the idealized wind stress: (a) zonal stress, and (b) meridional stress. Contour interval=0.2 N^2 m^{-4}.

Fig.7. The correlation between the wind stress predicted by the NN model and the idealized stress minus the correlation between the wind stress predicted by the LR model and the idealized wind stress, for: (a) zonal stress, and (b) meridional stress. Contour interval = 0.02. The zero contours are the dotted curves, while the negative contours are the dashed curves. Positive values means the NN predicted wind stress is outperforming the LR one.

Fig.8. The SSE of the NN wind stress minus the SSE of the LR wind stress, (both verified against the idealized wind stress), for: (a) zonal stress, and (b) meridional stress. Contour

interval=0.02 $N^2\ m^{-4}$. Negative values means the NN predicted wind stress is outperforming the LR one.

Fig.9. A comparison of the model SST between the ocean model driven by the FSU wind stress and that driven by the idealized stress (i.e. with only the first 3 EOFs), by (a) correlation (contour interval=0.1), and (b) RMS error (contour interval =0.2°C).

Fig.10. A cross-validated comparison of the ocean model SST between that driven by the idealized wind stress and that driven by the empirical wind stress from the NN model (with HC as predictors), by (a) correlation (contour interval=0.05), and (b) RMS error (contour interval=0.1°C).

Fig.11. The skill differences in the model SST between the model driven by the NN model wind stress and that driven by the LR model stress, with both model SSTs verified against the standard SST, i.e. the SST from the model driven by the idealized wind stress: (a) correlation skill difference (Contour interval = 0.02), and (b) RMS error difference (contour interval=0.02°C). Positive regions in (a) indicate NN ahead of LR, while negative region in (b) indicate NN ahead of LR.

Fig.12. Cross-validated skill differences in the model HC between the ocean model driven by NN model wind stress and that driven by the LR model stress, both verified against the model HC driven by the idealized wind stress: (a) correlation difference (contour interval = 0.02), (b) RMS error difference (contour interval=0.05°C). Positive regions in (a) indicate NN ahead of LR, while negative regions in (b) indicate NN ahead of LR.

Fig.13. Time evolution of observed SST anomalies in NINO3 (solid curve) and model HC averaged over 124°E-70°W,5°N-5°S (dashed curve) forced by the FSU observed wind stress. Both curves were normalised and smoothed by a 3-point running mean.

Table 1: Correlation between the observed SST and that from 10 models. The results of the first 9 models are taken from Palmer and Anderson(1994). The final model is the one used in this study. Model A, described in Wu et al (1994), is a $1\frac{1}{2}$ layer model with specified mean climatology. Model B, is a $2\frac{1}{2}$-layer model, described in Balmaseda et al (1994). Model C, described in Davey et al(1994), is also a $2\frac{1}{2}$-layer model. While model D and E are versions of the GFDL Modular Ocean Model, with resolution of $1\frac{1}{2}^o \times 1\frac{1}{2}^o$ and $\frac{1}{3}^o$ latitude $\times 1\frac{1}{2}^o$ longitude respectively.

Model	Region					
	EQ3	Niño4	EQ2	Niño3	EQ1	Niño1+2
Cane-Zebiak	–	0.46	–	0.60	–	0.68
Max-Planck Institute	–	0.76	–	0.74	–	0.59
OPYC	–	0.72	–	0.63	–	0.46
GFDL	–	0.81	–	0.69	–	0.57
A	0.43	0.64	0.77	0.73	0.69	0.54
B	0.27	0.59	0.77	0.75	0.69	0.40
C	0.34	0.55	0.67	0.62	0.51	0.26
D	0.60	0.76	0.79	0.55	0.55	0.54
E	0.59	0.76	0.79	0.65	0.60	0.58
Model used here	**0.55**	**0.73**	**0.82**	**0.80**	**0.75**	**0.38**

Table 2: Cross-validated correlation between the predicted wind stress EOF time series and the observed wind stress EOF time series for the first 3 modes, using the observed SST, the model SST, the model HC, and the model HC+SST as predictors. Results are shown for both the NN model and the LR model, and for the zonal (x) and meridional (y) components of the wind stress.

Predictors	Obs.SST		Mod.SST		HC		HC+SST	
Predictands	NN	LR	NN	LR	NN	LR	NN	LR
$\tau_x : \beta_1$	0.74	0.72	0.81	0.81	0.89	0.89	0.88	0.88
$\tau_x : \beta_2$	0.57	0.52	0.54	0.52	0.76	0.73	0.75	0.70
$\tau_x : \beta_3$	0.38	0.24	0.11	0.06	0.40	0.35	0.29	0.26
$\tau_y : \beta_1$	0.86	0.83	0.83	0.81	0.86	0.86	0.84	0.86
$\tau_y : \beta_2$	0.53	0.43	0.47	0.46	0.66	0.66	0.57	0.62
$\tau_y : \beta_3$	0.47	0.45	0.21	0.19	0.24	0.21	0.28	0.24

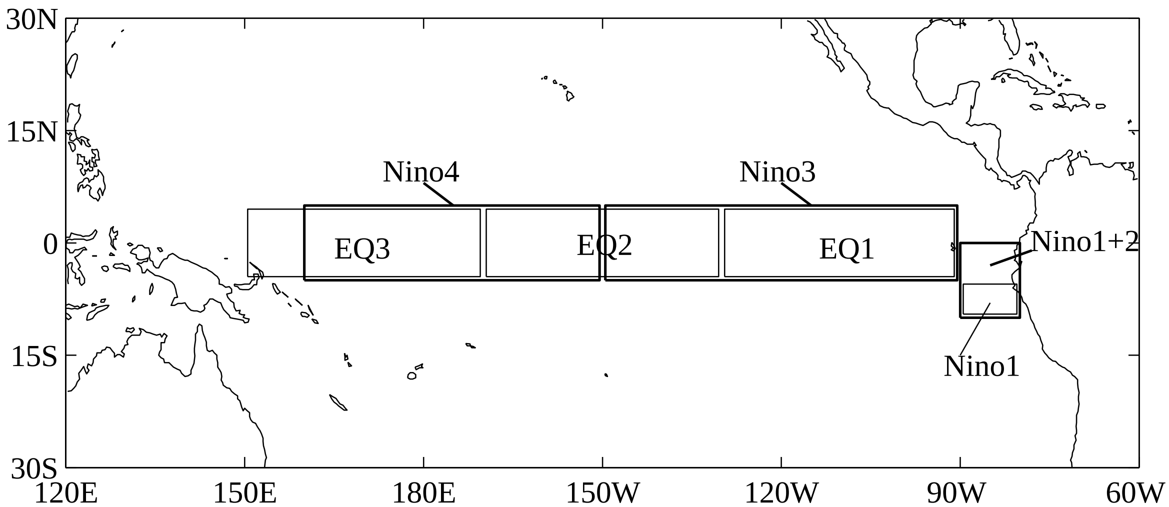

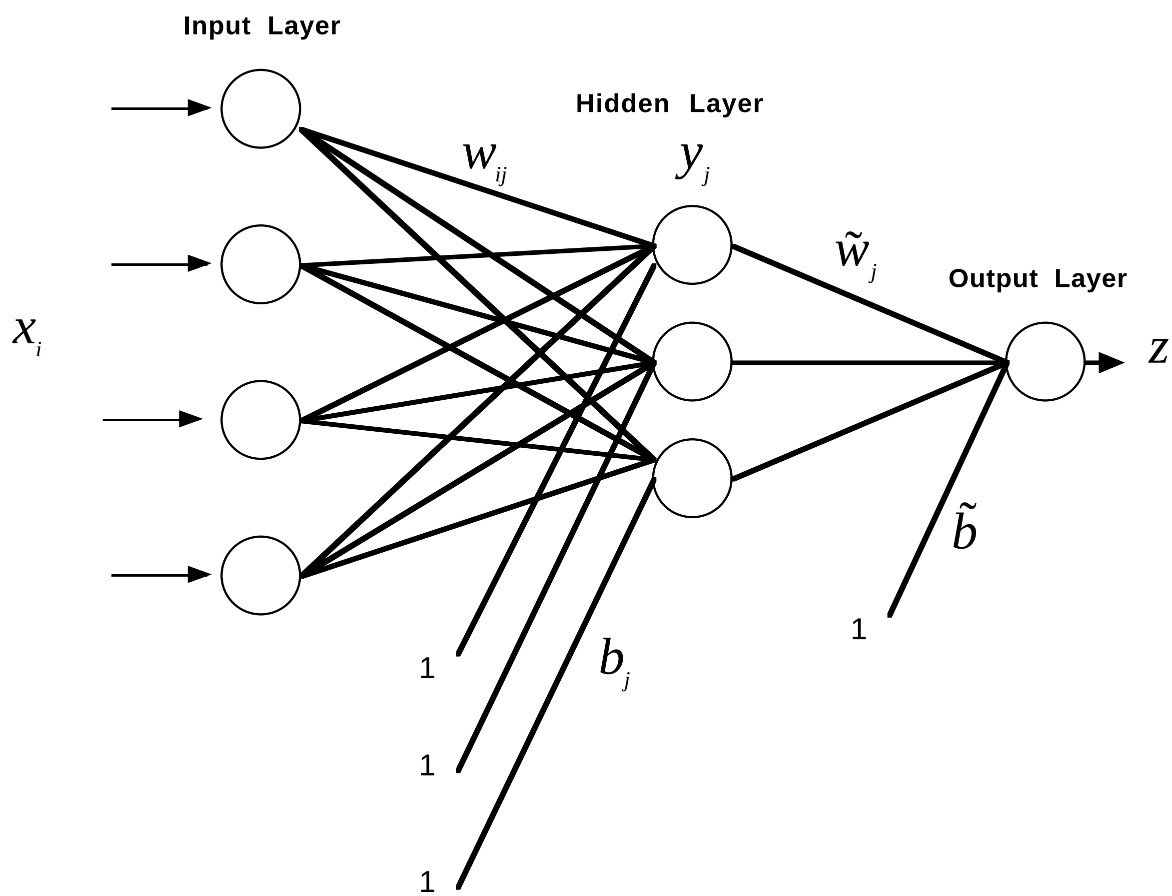
Input Layer
Hidden Layer
Output Layer
x_i
w_{ij}
y_j
$\tilde{w}_j$
z
$\tilde{b}$
b_j
1
1
1
1

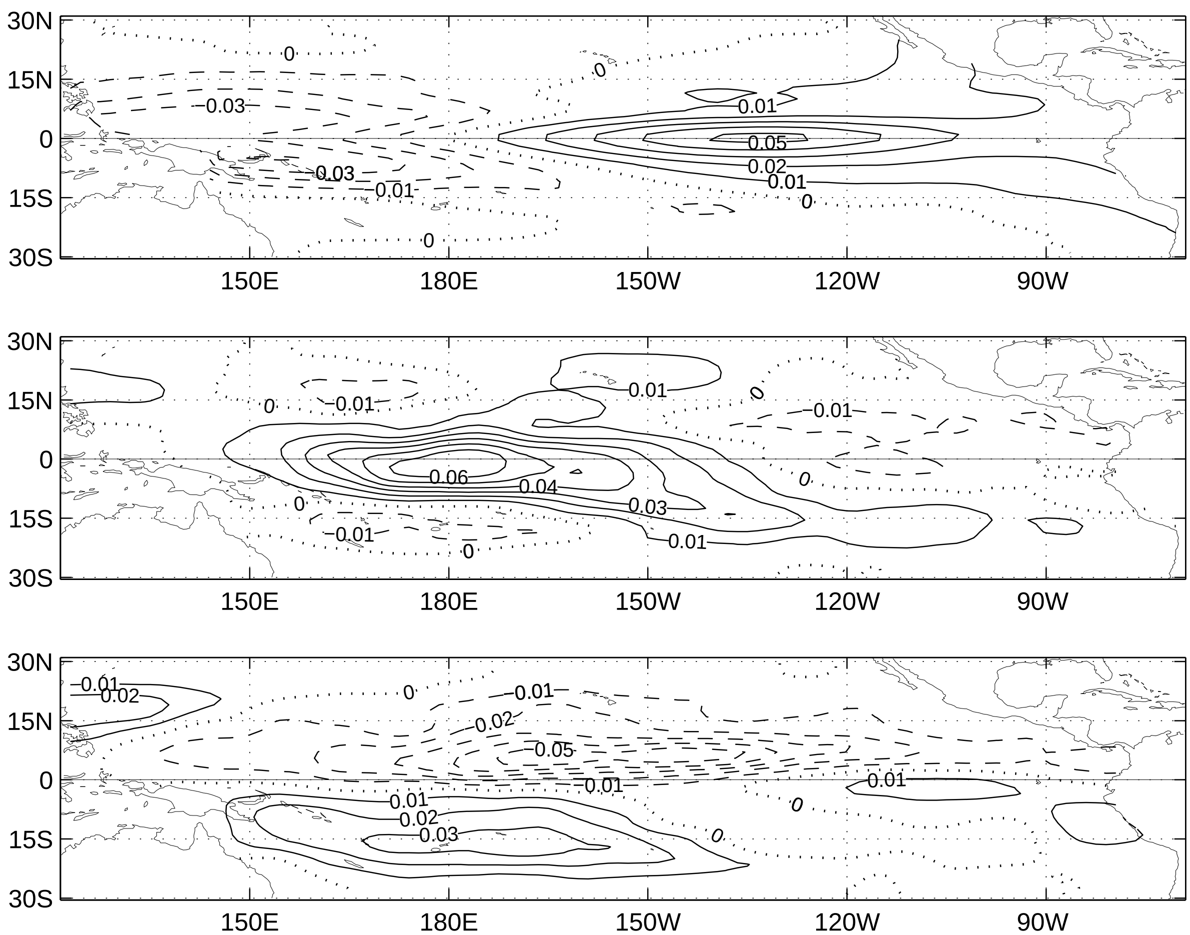
30N
15N
0
15S
30S
150E
180E
150W
120W
90W
0
0.01
0.02
0.03
0.04
0.05
0.06

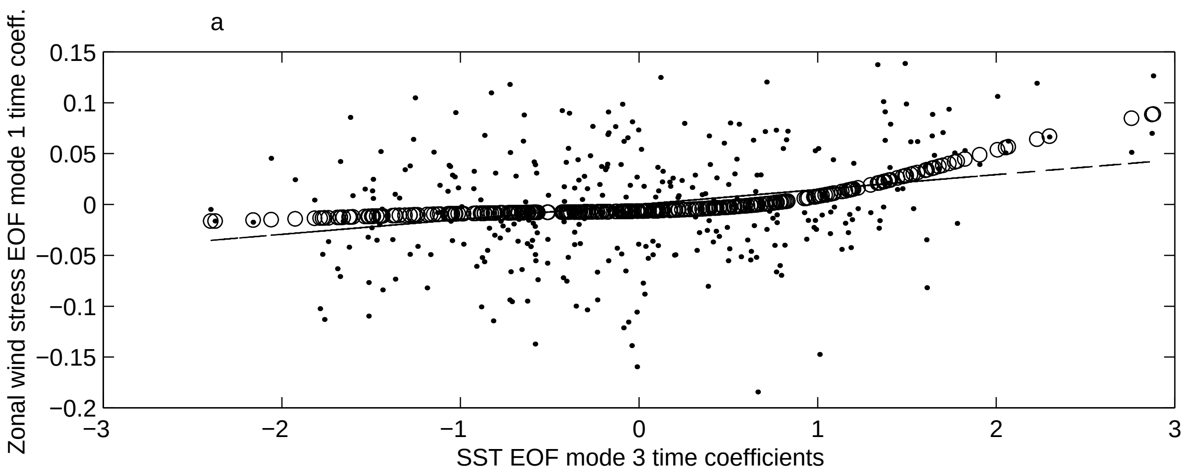
a
0.15
0.1
0.05
0
−0.05
−0.1
−0.15
−0.2
−3
−2
−1
0
1
2
3
Zonal wind stress EOF mode 1 time coeff.
SST EOF mode 3 time coefficients

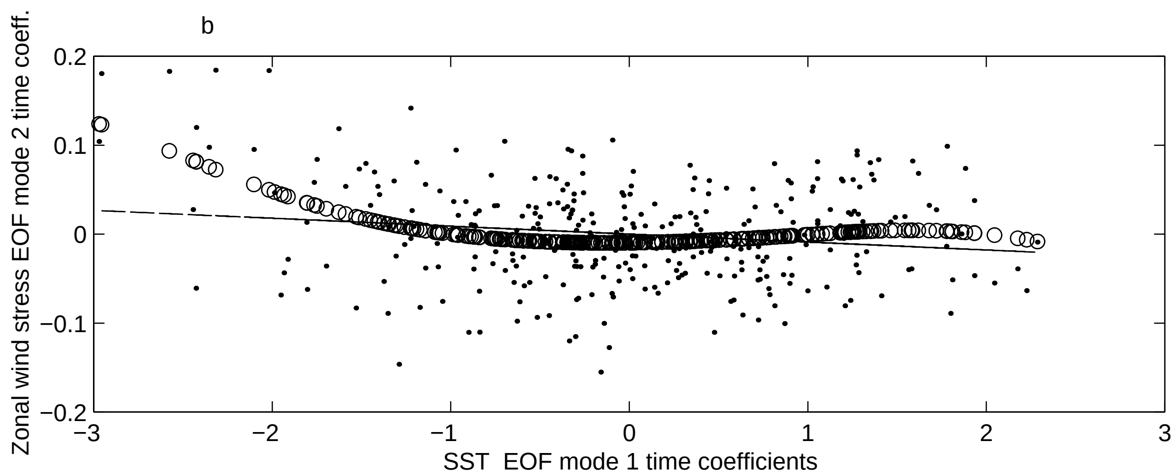
b
0.2
0.1
0
−0.1
−0.2
−3
−2
−1
0
1
2
3
Zonal wind stress EOF mode 2 time coeff.
SST EOF mode 1 time coefficients

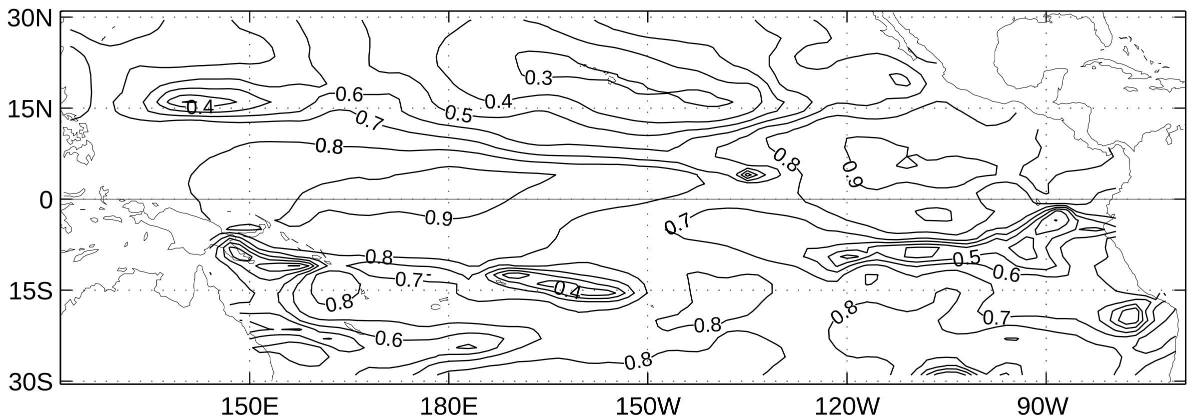
30N
15N
0
15S
30S
150E
180E
150W
120W
90W
0.3
0.4
0.4
0.5
0.6
0.7
0.8
0.9
0.8
0.9
0.7
0.8
0.7
0.4
0.8
0.6
0.8
0.8
0.8
0.5
0.6
0.7
0.8

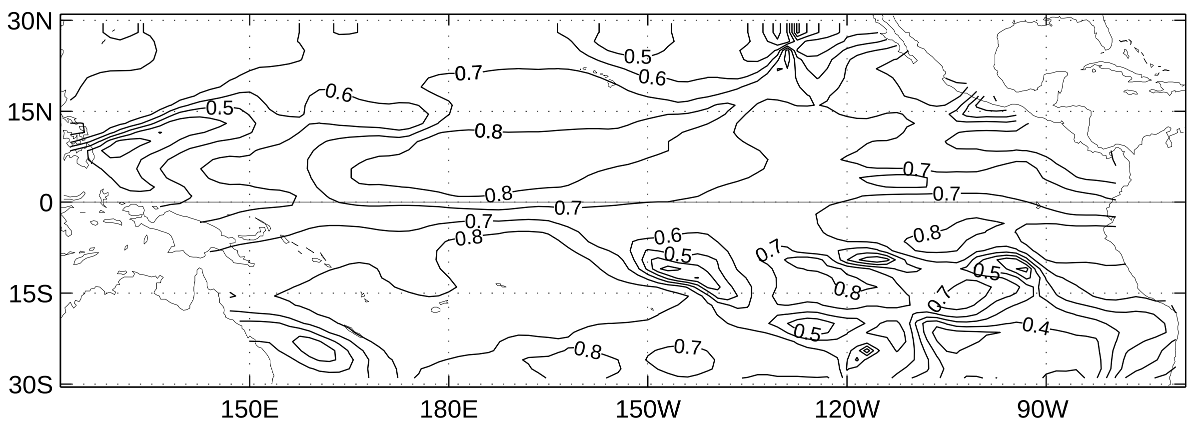
30N
15N
0
15S
30S
150E
180E
150W
120W
90W
0.5
0.7
0.6
0.6
0.5
0.8
0.8
0.7
0.7
0.7
0.7
0.8
0.6
0.5
0.7
0.8
0.8
0.5
0.7
0.5
0.4
0.8
0.7

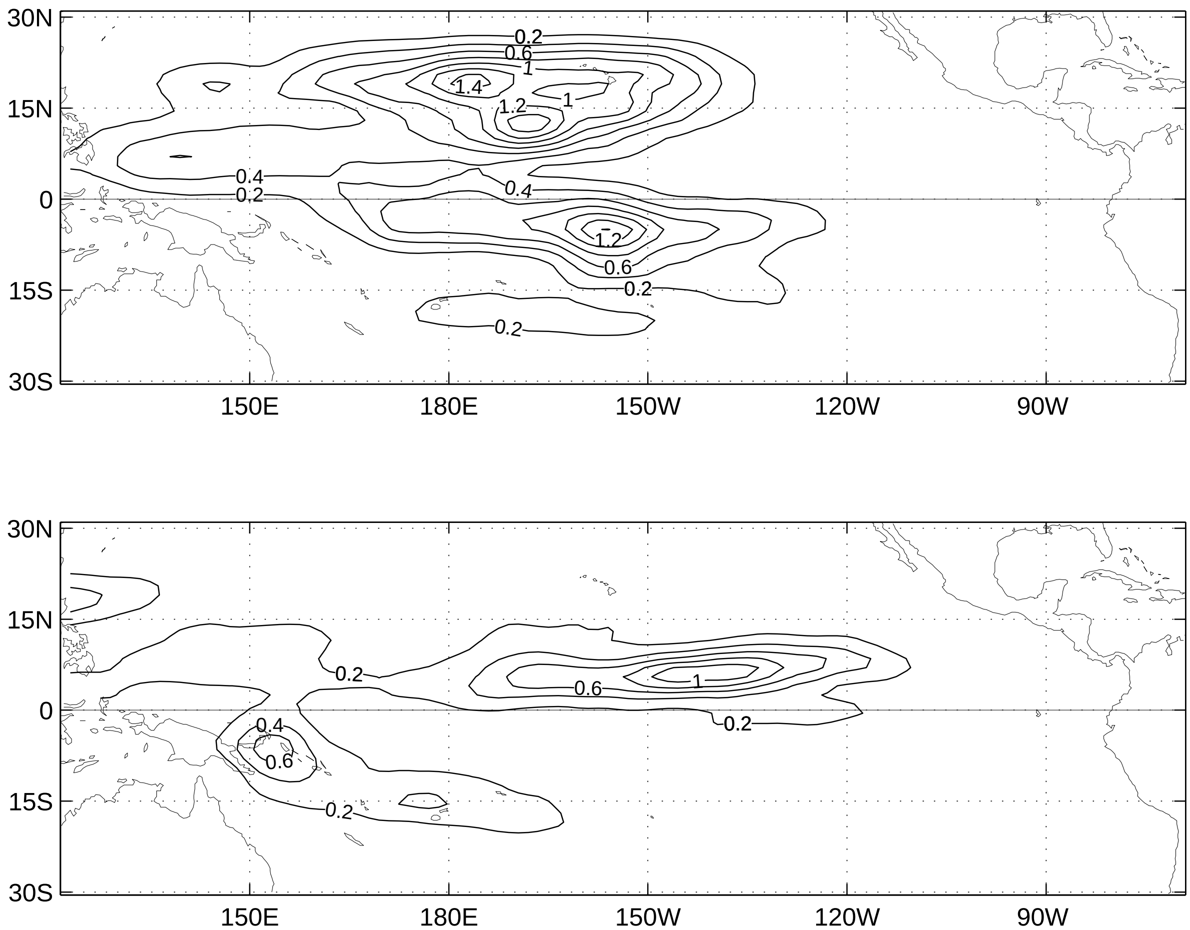
30N
15N
0
15S
30S
150E
180E
150W
120W
90W
0.2
0.6
1
1.4
1.2
1
0.4
0.2
0.4
1.2
0.6
0.2
0.2
30N
15N
0
15S
30S
150E
180E
150W
120W
90W
0.2
0.6
1
0.2
0.4
0.6
0.2

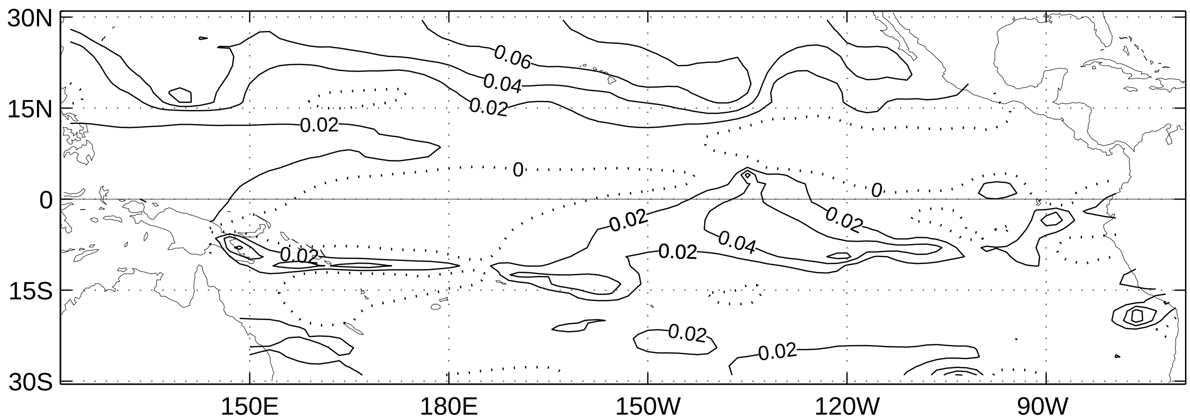
30N
15N
0
15S
30S
150E
180E
150W
120W
90W
0.06
0.04
0.02
0

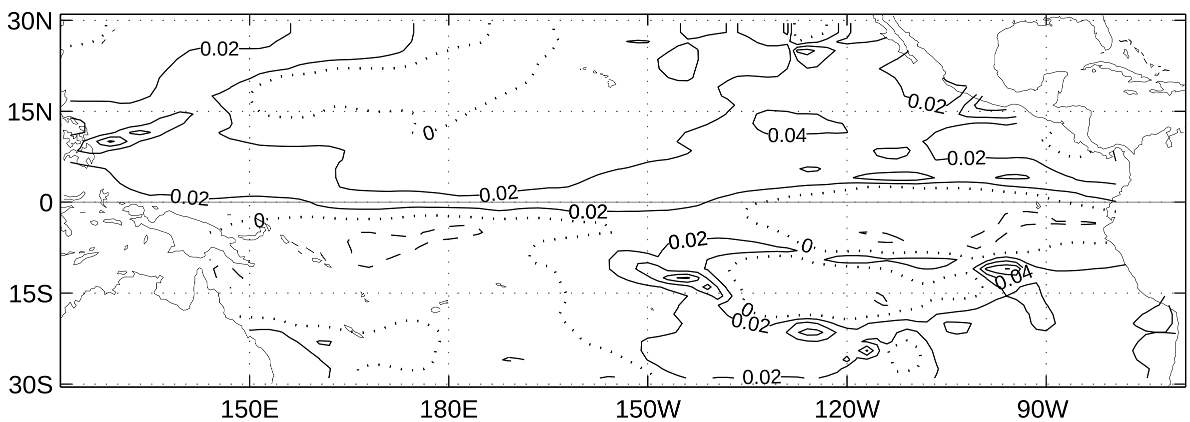
30N
15N
0
15S
30S
150E
180E
150W
120W
90W
0.02
0.04
0

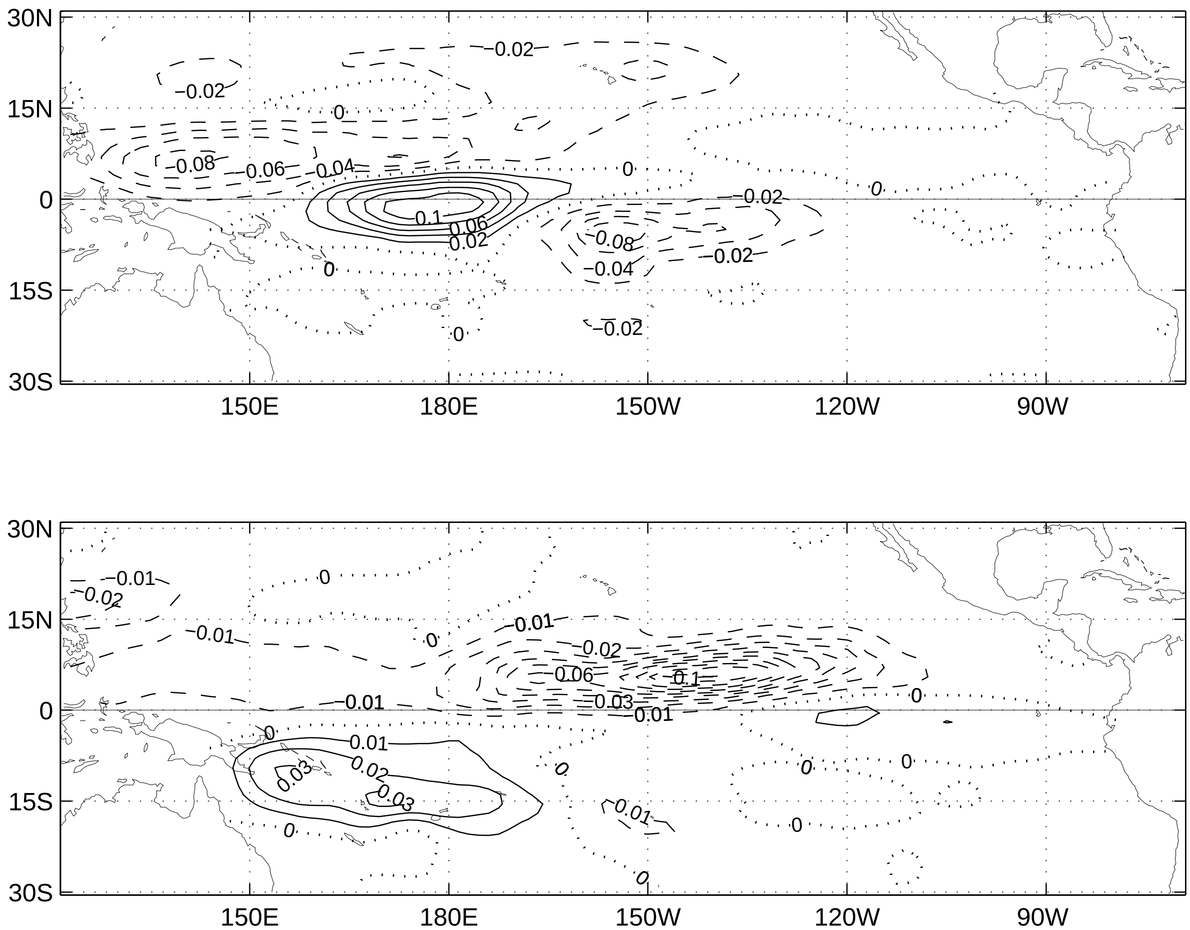
30N
15N
0
15S
30S
150E
180E
150W
120W
90W
30N
15N
0
15S
30S
150E
180E
150W
120W
90W

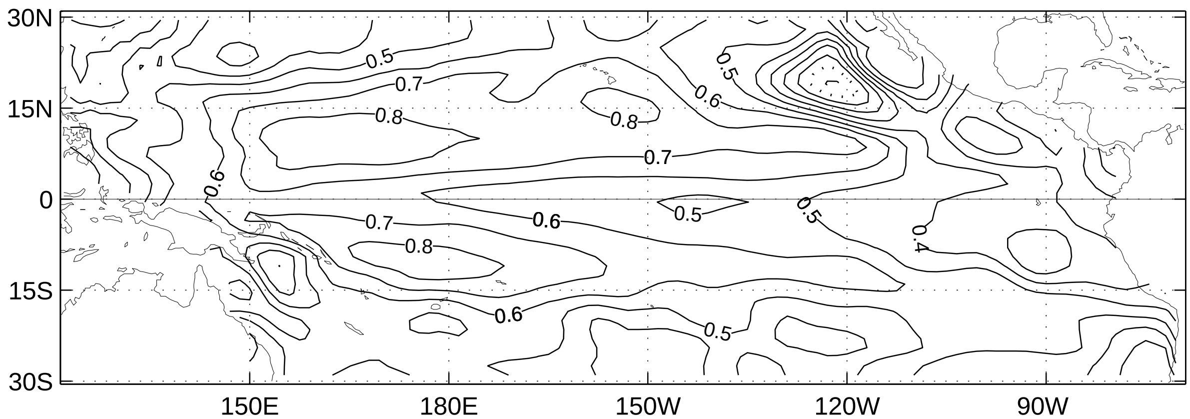
30N
15N
0
15S
30S
150E
180E
150W
120W
90W
0.5
0.7
0.8
0.6
0.4

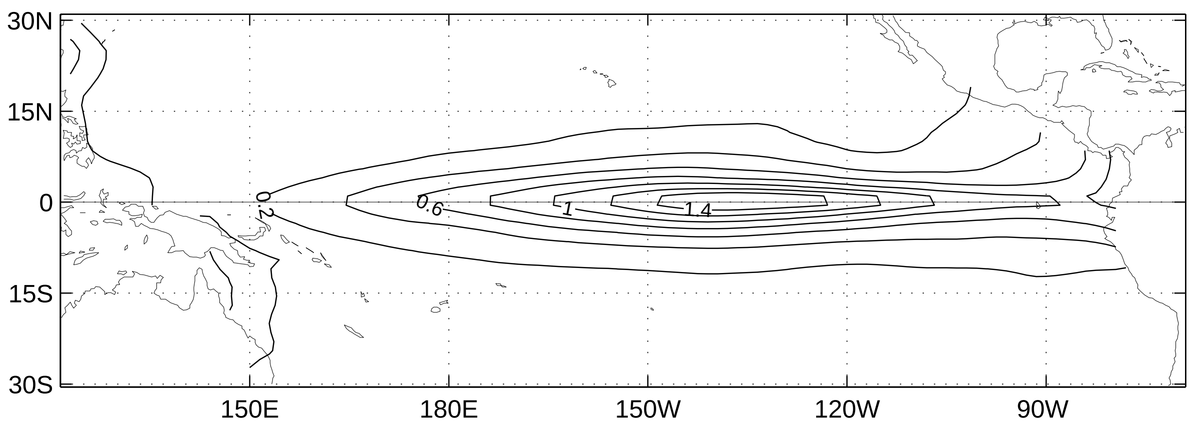
30N
15N
0
15S
30S
150E
180E
150W
120W
90W
0.2
0.6
1
1.4

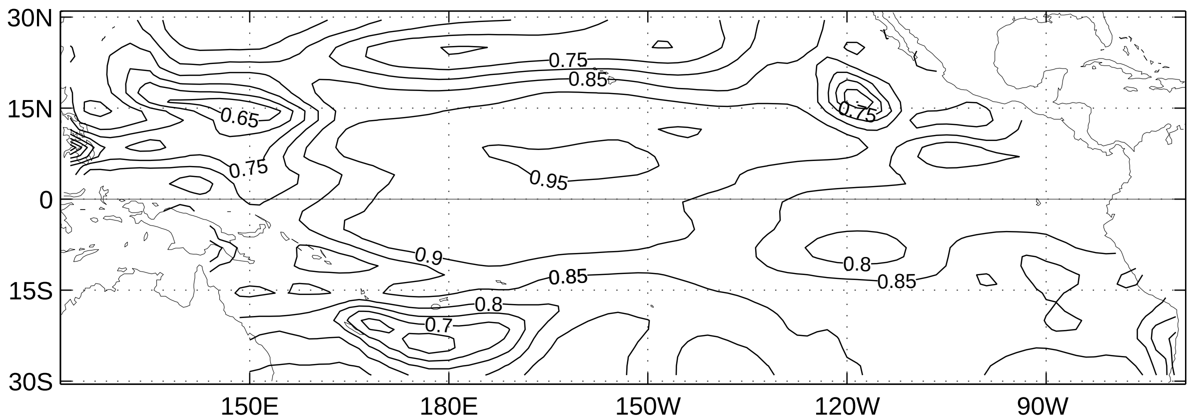
30N
15N
0
15S
30S
150E
180E
150W
120W
90W
0.75
0.85
0.65
0.75
0.95
0.75
0.9
0.85
0.8
0.7
0.8
0.85

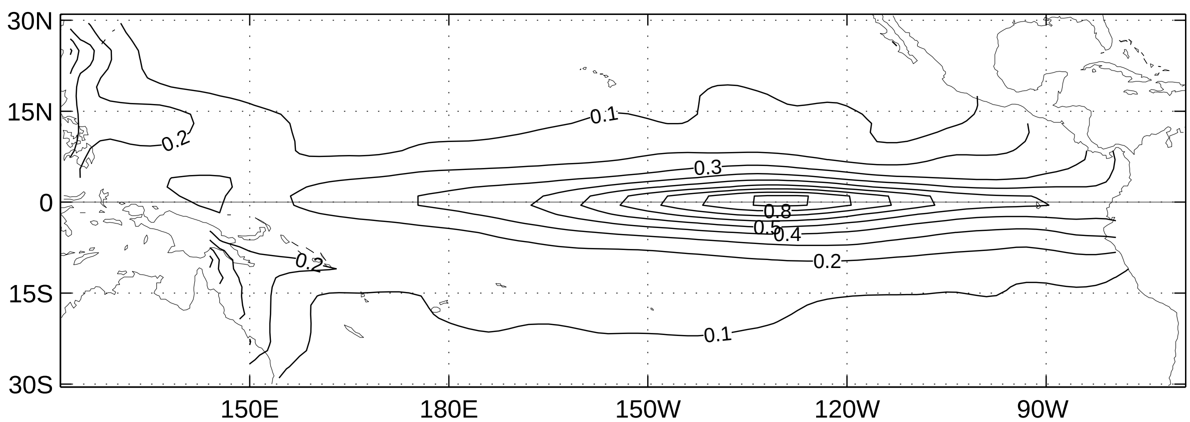
30N
15N
0
15S
30S
150E
180E
150W
120W
90W
0.1
0.2
0.3
0.8
0.5
0.4
0.2
0.2
0.1

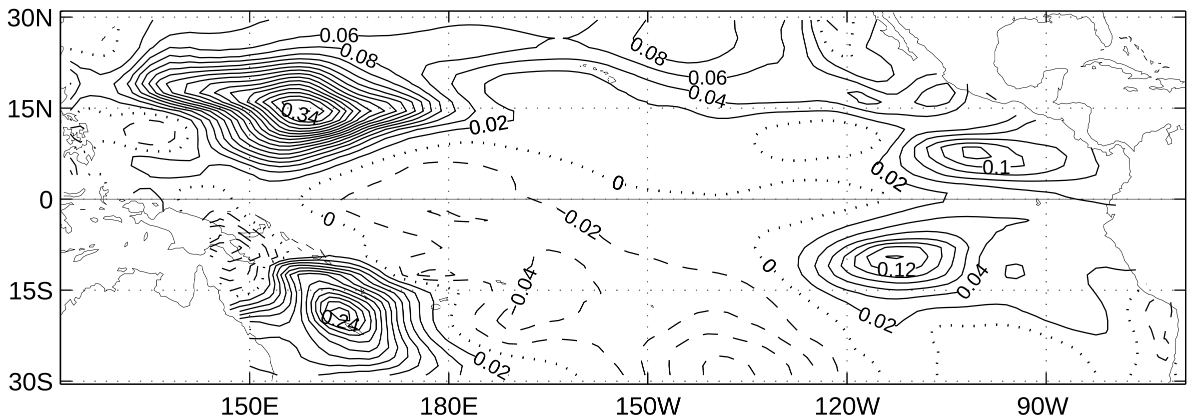
30N
15N
0
15S
30S
150E
180E
150W
120W
90W
0.06
0.08
0.34
0.02
0
0.1
0.12
0.04
0.24

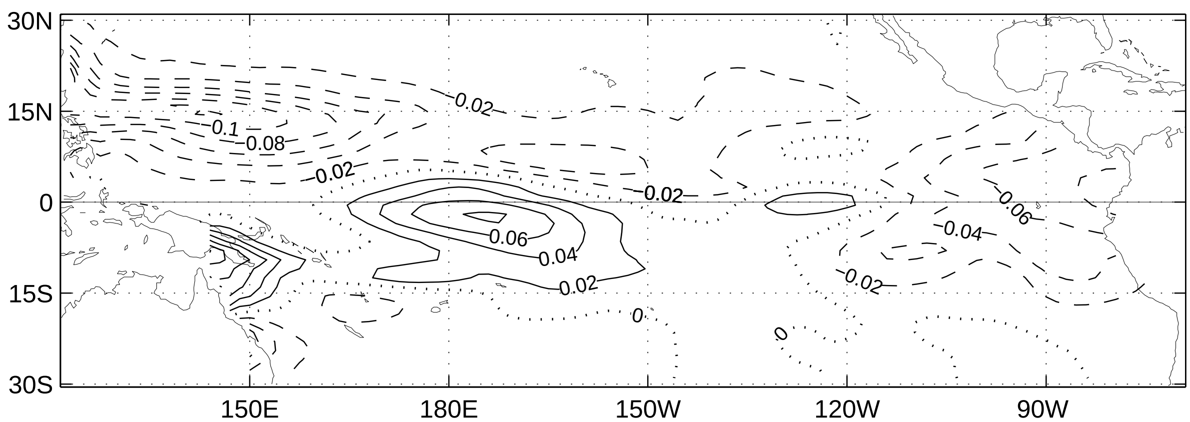
30N
15N
0
15S
30S
150E
180E
150W
120W
90W
0.02
0.1
0.08
0.06
0.04
0

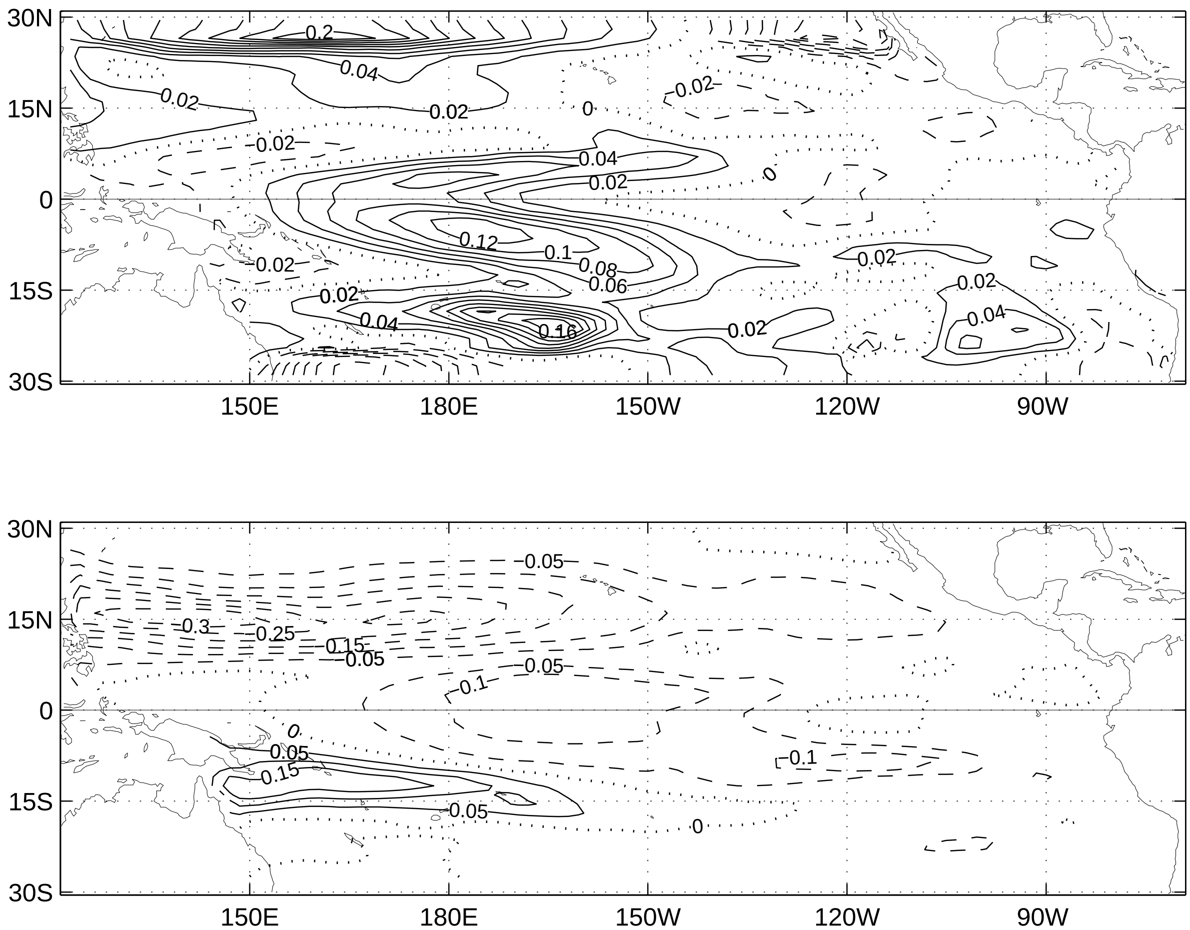
30N
15N
0
15S
30S
150E
180E
150W
120W
90W
0.2
0.04
0.02
0.02
0
0.02
0.02
0.04
0.02
0
0.12
0.1
0.08
0.06
0.02
0.02
0.02
0.02
0.04
0.16
0.02
0.04
30N
15N
0
15S
30S
150E
180E
150W
120W
90W
0.05
0.3
0.25
0.15
0.05
0.05
0.1
0
0.05
0.15
0.1
0.05
0

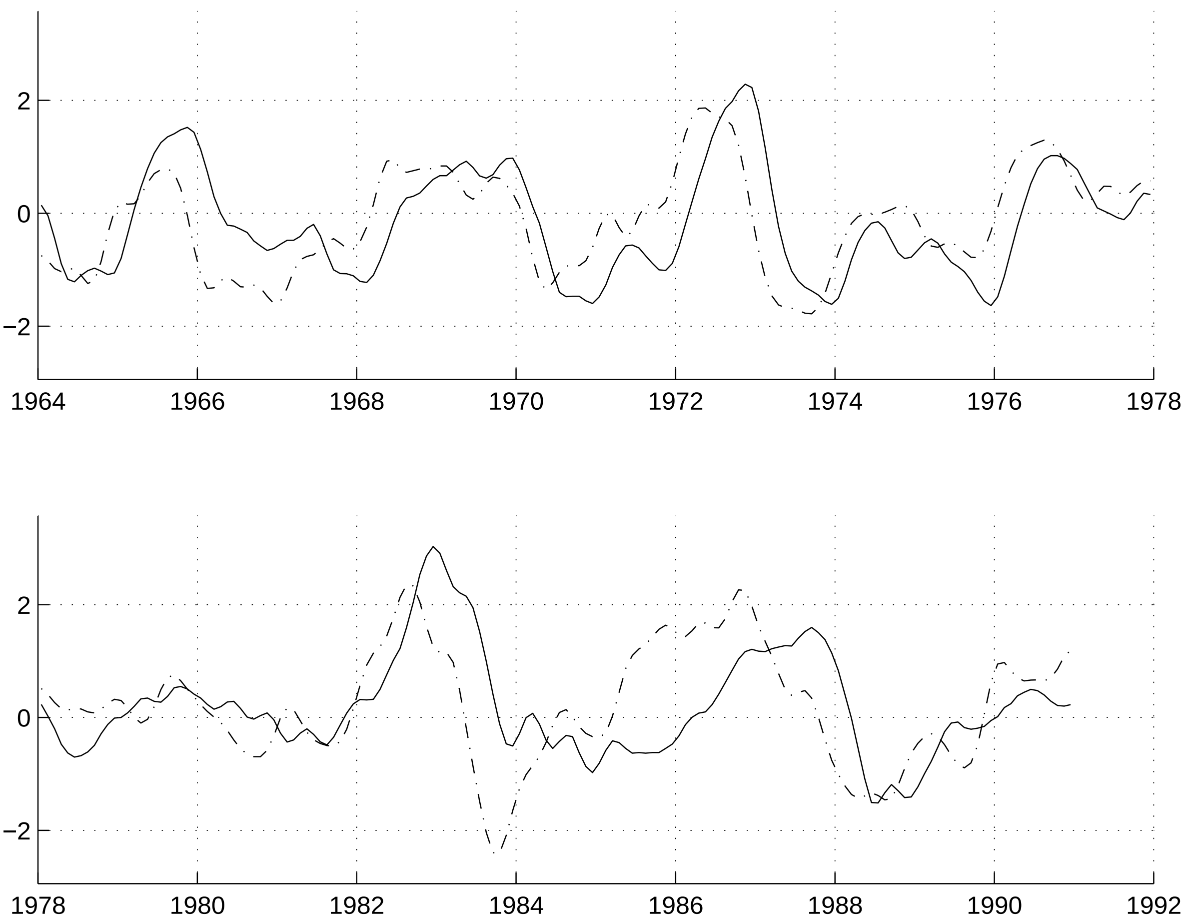

max=3.0336, min=−2.4017